A DISTANCE ESTIMATE TO THE CYGNUS LOOP
BASED ON THE DISTANCES TO TWO STARS LOCATED WITHIN THE REMNANT

Robert A. Fesen, Jack M. M. Neustadt, Christine S. Black

6127 Wilder Lab, Department of Physics & Astronomy, Dartmouth College, Hanover, NH 03755, USA

AND

Dan Milisavljevic

Harvard-Smithsonian Center for Astrophysics, Cambridge, MA 02138, USA

Department of Physics and Astronomy, Purdue University, 525 Northwestern Avenue, West Lafayette, IN 47907, USA

ABSTRACT

Underlying nearly every quantitative discussion of the Cygnus Loop supernova remnant is uncertainty about its distance. Here we present optical images and spectra of nebulosities around two stars whose mass-loss material appears to have interacted with the remnant's expanding shock front and thus can be used to estimate the Cygnus Loop's distance. Narrow passband images reveal a small emission-line nebula surrounding an M4 red giant near the remnant's eastern nebula NGC 6992. Optical spectra of the nebula show it to be shock-heated with significantly higher electron densities than seen in the remnant's filaments. This along with a bow-shaped morphology suggests it is likely red giant mass-loss material shocked and accelerated by passage of the Cygnus Loop's blast wave. We also identify a B7 V star located along the remnant's northwestern limb which also appears to have interacted with the remnant's shock wave. It lies within a small arc of nebulosity in an unusually complex region of highly curved and distorted filaments along the remnant's northern shock front suggestive of a localized disturbance of the shock front due to the B star's stellar winds. Based on the assumption that these two stars lie inside the remnant, combined with an estimated distance to a molecular cloud situated along the remnant's western limb, we propose a distance to the Cygnus Loop of 1.0 ± 0.2 kpc. Although larger than several recent estimates of $500 - 800$ pc, a distance $\simeq 1$ kpc helps resolve difficulties with the remnant's postshock cosmic ray and gas pressure ratio and estimated supernova explosion energy.

Subject headings: ISM: individual (Cygnus Loop) - ISM: kinematics and dynamics - ISM: supernova remnants

1. INTRODUCTION

The Galactic supernova remnant G74.0-8.5, commonly known as the Cygnus Loop, Veil Nebula or Network Nebula is widely considered to be a prototypical middle-age remnant with an estimated age of $1 - 2 \times 10^4$ yr ((Cox 1972; McCray & Snow 1979; Miyata et al. 1994; Levenson et al. 1998)). Discovered by William Herschel in 1784, the remnant consists of a limb-brightened shell 2.8×3.5 degrees in angular size.

The remnant is composed of several bright optical nebulosities including NGC 6960, NGC 6974, NGC 6979, NGC 6992, NGC 6995, IC 1340, plus a large but fainter nebulosity in the remnant's northwestern region known as Pickering's Triangle. The near circular arrangement of these nebulae, referred to as the Cygnus loop by early observers, quickly led to suspicions of it being a supernova remnant (Zwicky 1940; Oort 1946; Walsh & Hanbury Brown 1955).

The remnant's large angular size, relative brightness across many wavelengths, plus little foreground extinction due to its location more than eight degrees off the Galactic plane ($E(B - V) = 0.05 - 0.15$; Raymond et al. (1981)) has made it one of the best studied Galactic supernova remnants. Exhibiting an extensive and well resolved filamentary structure, it has been shown to be an excellent laboratory for investigating various shock processes including shock–cloud interactions, X-ray, UV, and optical emissions from pre- and post-shock plasma, and interstellar grain destruction.

Based on analysis of X-ray, UV, optical, and radio observations and modeling, the Cygnus Loop appears best understood as a remnant of a supernova explosion which occurred inside an interstellar cavity created by winds off a high-mass progenitor star (McCray & Snow 1979; Ciotti & D'Ercole 1989; Hester et al. 1994; Levenson et al. 1997, 1998; Miyata & Tsunemi 1999).

X-ray emission seen near the remnant's projected centre shows a metal-rich plasma suggesting ejecta from a type II core-collapse event (Miyata et al. 1998). In addition, X-ray emissions from certain regions along northeast and southwest limbs have relatively high metal abundances also suggesting a high-mass, core-collapse supernova (Tsunemi et al. 2007; Katsuda et al. 2008; Kimura et al. 2009; Uchida et al. 2009; Fujimoto et al. 2011; Katsuda et al. 2011).

Hubble (1937) measured a proper motion of $0.''03$ yr^{-1} of the bright eastern and western nebulae away from the centre of expansion. This proper motion, when combined with an observed radial velocity of 115 km s^{-1} for 25 of the remnant's optical filaments, led to the first distance estimate for the Cygnus Loop of 770 pc (Minkowski 1958).

Subsequent distance estimates have varied considerably with the full range of possible distances taking into account measurement uncertainties being 300 and 1800 pc (see Table 1). One of the most cited values is 576 ± 61 pc made by Blair et al. (2009) who used the presence

TABLE 1
Distance Estimates to the Cygnus Loop

Reference	Distance	Range	Method
Minkowski (1958)	770 pc	$\cdots$	bright optical filament velocities and proper motions
Rappaport et al. (1974)	770 pc	$470 - 1070$ pc	shock velocity from X-ray data analysis
Sakhibov & Smirnov (1983)	1400 pc	$1000 - 1800$ pc	optical filament velocities and proper motions
Braun & Strom (1986)	460 pc	$300 - 620$ pc	bright optical filament velocities and proper motions
Hester et al. (1986)	700 pc	$500 - 1000$ pc	Balmer filament proper motion + assumed shock velocity
Shull & Hippelein (1991)	600 pc	$300 - 1200$ pc	Fabry Perot scan velocities and filament proper motions
Blair et al. (1999)	440 pc	$340 - 570$ pc	Balmer filament proper motion + modeled shock velocity
Blair et al. (2005)	570 pc	$460 - 670$ pc	Balmer filament proper motion + modeled shock velocity
Blair et al. (2009)	576 pc	$510 - 637$ pc	UV spectrum of a background sdOB star
Salvesen et al. (2009)	640 pc	$422 - 960$ pc	ratio of cosmic ray to gas pressure in post-shock region
Medina et al. (2014)	890 pc	$790 - 1180$ pc	Hα line widths & proper motions
Raymond et al. (2015)	800 pc	$\cdots$	revised distance estimate of Medina et al. (2014)
This work	1000 pc	$800 - 1200$ pc	distance estimates to two stars located inside the remnant

of O VI 1032 Å line absorption in the spectrum of a sdOB star lying in the direction to Cygnus Loop's eastern NGC 6992 nebulosity. However, more recent distance estimates have tended to favor numbers closer to Minkowski's original 770 pc value.

Here we report on a distance measurement to the Cygnus Loop based on estimated distances to two stars which we suspect lie inside the remnant. These stars have surrounding stellar mass loss nebulae which have properties suggestive of an interaction with the remnant's expanding shock front. If these stars do in fact lie within the remnant, then one can use spectroscopic parallax on these stars to deduce the Cygnus Loop's true distance.

One star is a V = 11.6 magnitude red giant at α[J2000] = $20^h56^m0.935^s$, δ[J2000] = $+31^o31'29''.74$, henceforth referred to as J205601. It has a projected location near the remnant's bright eastern nebulosity, NGC 6992, and appears centred within a small optical nebula quite distinct in morphology from the remnant's other eastern limb emission features.

This star and its surrounding nebulosity came to our attention via a color image of the Cygnus Loop featured as "Astronomy Picture of the Day" for 1 December 2009 taken by Daniel Lopez[1] using the 2.5m Isaac Newton Telescope at Roque de los Muchachos Observatory. The star's nebulosity is relatively faint, only weakly seen in the broad band Digital Sky Survey (DSS) images, and not readily apparent even in narrow interference filter images taken of the remnant (Levenson et al. 1998).

A second star, BD+31 4224, is a V = 9.58 magnitude late B star located near the remnant's northwestern limb (α[J2000] = $20^h47^m51.817^s$, δ[J2000] = $+32^o14'11.33''.74$). It was found during a follow-up search for additional stars projected with the remnant's boundaries that exhibited possible evidence for CSM interaction with the Cygnus Loop's shock. This star lies within a small arc of nebulosity in an unusually complex region of curved and distorted filaments along the remnant's northwestern boundary suggestive of a localized disturbance in the remnant's shock front.

The projected locations of these two stars in the Cygnus Loop are shown in Figure 1. Our optical imaging and spectral observations on both stars and the nature of surrounding nebulosities in regard to possible physical connections to the Cygnus Loop are described in §2 and

§3. The stars' use as distance indicators of the remnant is discussed in §4 with our conclusions concerning the likely distance to the Cygnus Loop summarized in §5.

2. OBSERVATIONS

2.1. *Images*

Narrow passband images of the nebulosity around J205601 were first obtained in September 2011 using a 4096 x 4096 Lawrence-Berkeley National Labs red sensitive CCD mounted on the 2.4m telescope at the MDM Observatory at Kitt Peak Arizona. To increase the signal-to-noise of the images, we employed 4×4 on-chip binning which resulted in an image scale of $0''.676$ per pixel.

Images were taken using an Hα filter (FWHM = 30 Å), a [S II] 6716, 6731 Å filter (FWHM = 50 Å), and an [O III] 5007 Å filter (FWHM = 50 Å). Three or four 600 s exposures of the nebulosity were taken in each filter along with twilight sky flats. Due to the size of the filters used, the effective image field was 8.5×8.5 arcminutes. Standard data reduction of the images was performed using IRAF/STSDAS[2]. This included debiasing, flat-fielding, and cosmic ray and hot pixel removal.

Images of nebulosities around J205601 and BD+31 4224 were obtained in June 2012 and October 2014 using the 1.3m McGraw-Hill telescope at MDM Observatory at Kitt Peak, AZ. These images were taken using a 1k × 1k SITe CCD and 2×2 pixel on-chip binning yielding a image scale of 1.06 arcsec per pixel. A series of narrow passband [S II] (FWHM = 80 Å) and [O III] (FWHM = 50 Å) exposures with exposure times of 4×600 s.

Additional narrow passband images were taken with the MDM 2.4m telescope in September 2014 using a 2048×2048 pixel SITe CCD detector with a resolution $0''.508$ pixel^{-1}. For J205601, two 1000 s exposures were taken with an Hα filter (FWHM = 80 Å). For BD+31 4224, two 600 s exposures were taken for three nearby regions which were mosaiced into a larger image with a field-of-view of $\approx 24'$. Finally, photometric B and V observations were obtained in May 2017 using the 1.3m

[1] Instituto de Astrofisica de Canarias

[2] IRAF is distributed by the National Optical Astronomy Observatories, which is operated by the Association of Universities for Research in Astronomy, Inc. (AURA) under cooperative agreement with the National Science Foundation. The Space Telescope Science Data Analysis System (STSDAS) is distributed by the Space Telescope Science Institute.
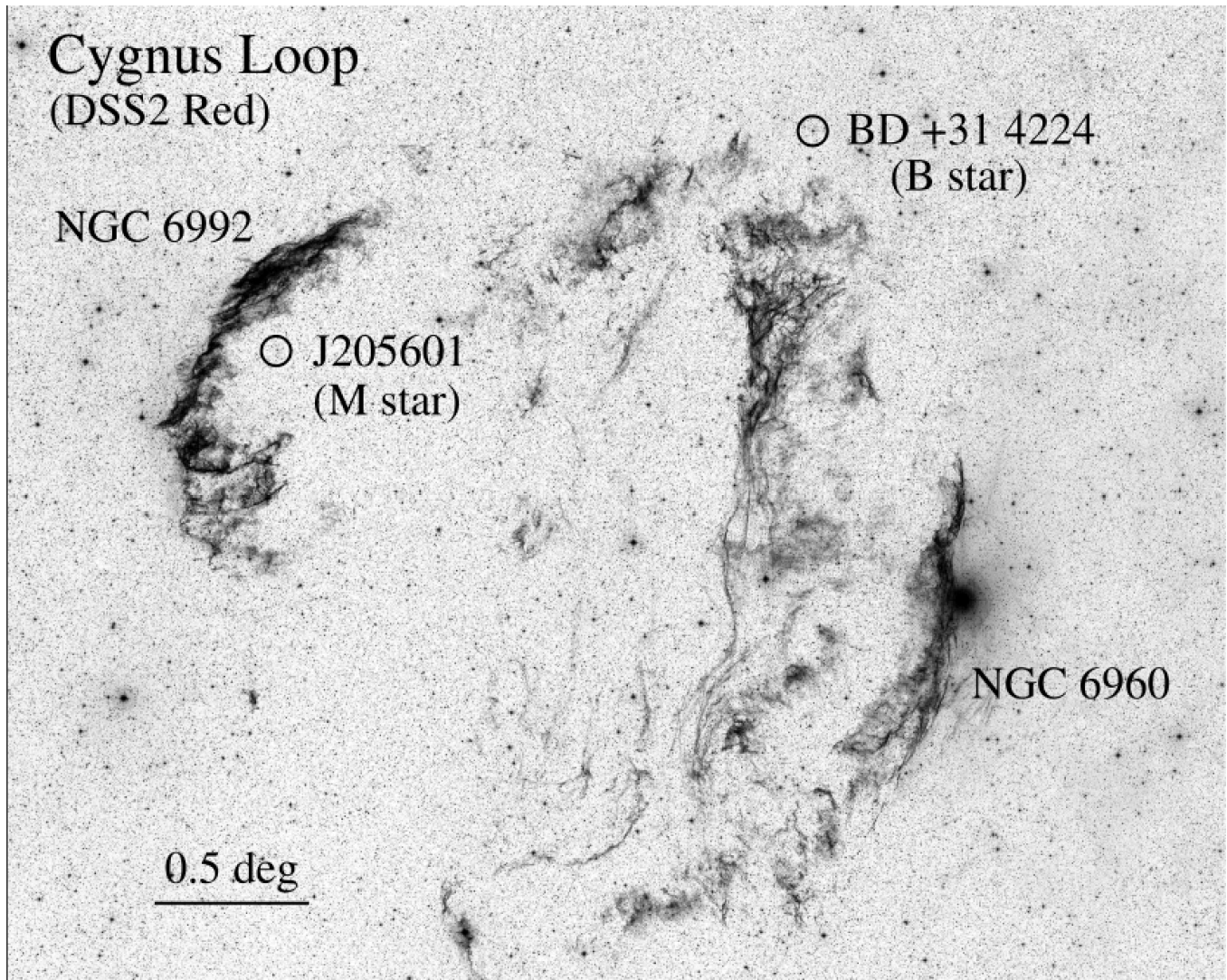
FIG. 1.— Reproduction of the red image of the Digital Sky Survey of the Cygnus Loop. Marked are the two stars (J205601+313130 and BD+31 4224) which we suspect of lying inside the remnant. North is up, East to the left.

MDM telescope and a 1k × 1k SITe CCD. Photometric calibration observations were taken of +50 declination standard stars (Landolt 2013) observed at air masses close to those for J205601 and BD+31 4224.

2.2. Spectra

Low-resolution optical spectra were taken in October 2011 using the Multi-Aperture Red Spectrometer (MARS) attached to the 4m telescope at Kitt Peak National Observatory. A 1.2" × 5′ slit was used with a 450 g/mm VPH grating to yield a resolution of 10 Å and a wavelength coverage of $5500 - 10800$ Å. Spectra were obtained using east-west slits.

Low-dispersion 4000-7400 Å spectra of the filaments surrounding BD+31 4224 were obtained in October 2012 using the Boller & Chivens CCD spectrograph at the 2.4m Hiltner telescope at MDM Observatory. The spectrograph delivered a of 3.29 Å pixel^{-1} with a 1.0″ slit, resulting in a spectral resolution of 12 Å.

We also obtained spectra of BD+31 4224 and J205601 in October 2015 using the 2.4m Hiltner telescope using the OSMOS Spectrograph (Martini et al. 2011) and a blue Grism with resolutions of 0.7 Å pixel^{-1}. The spectra covered 3900–6800 Å with a spectral resolution of 1.2 Å pixel^{-1}.

We performed standard pipeline data reduction using IRAF. The images were bias-subtracted, flat-field corrected using twilight sky flats, and averaged to remove cosmic rays and improve signal-to-noise. Spectra were similarly reduced using IRAF and the software L.A. Cosmic to remove cosmic rays. The spectra were calibrated using quartz and Ar lamps and spectroscopic standard stars (Oke 1974; Massey & Gronwald 1990). Relative line strengths are believed accurate to better than 10% for the stronger emission lines.

3. RESULTS

Below we present spectral and imaging data on two stars which we suspect lie physically inside the Cygnus Loop remnant based on evidence suggesting interactions of these stars' mass loss material with the remnant's shock front in the form of surrounding optical nebulosities.

TABLE 2
Stars Suspected to Lie Inside the Cygnus Loop

| Star | Magnitudes[a] | | | | | Spectral | M_V | Distance[b] |
ID	B	V	J	H	K	Type	(mag)	(kpc)
J205601[c]	13.08 ± 0.30	11.57 ± 0.12	7.088 ± 0.026	6.136 ± 0.02	5.834 ± 0.02	M4 III	+1.0 to −2.0	1.0 - 4.6
BD+31 4224	9.53 ± 0.02	9.58 ± 0.02	9.709 ± 0.02	9.763 ± 0.02	9.791 ± 0.02	B7 V-IV	−0.1 to −1.3	0.8 - 1.3

[a] Magnitudes are taken from the Tycho-2 and 2MASS Catalogs.
[b] Distances calculated assuming $A_V = 0.25$
[c] Alternate ID: TYC 2688-1037-1
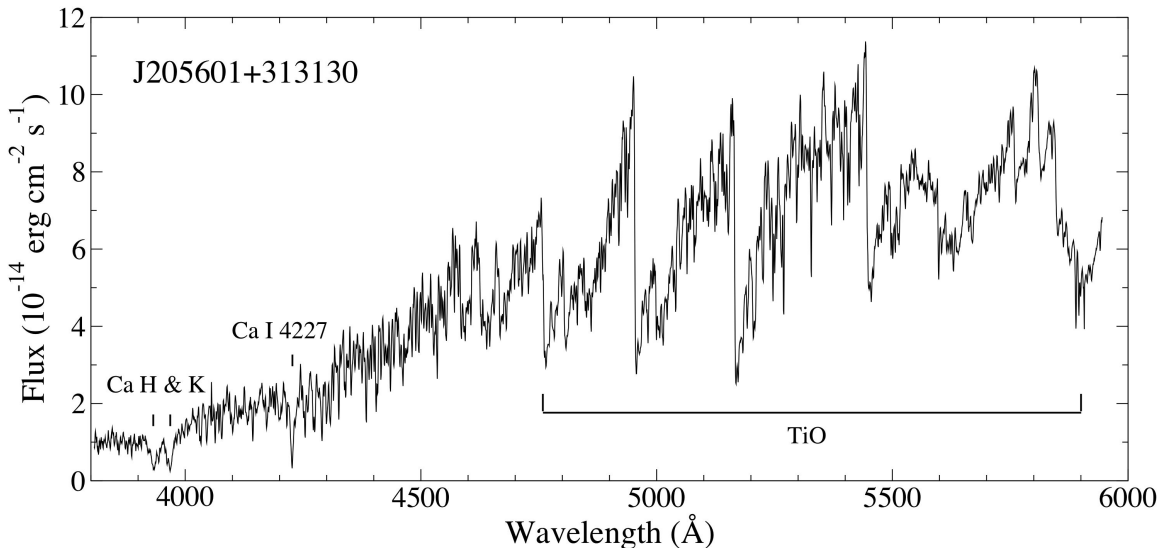
Fig. 2.— Low dispersion optical spectra of the M star J205601+313130.

3.1. *J205601: A M4 III Inside a Bow-Shock Nebula*
3.1.1. *Stellar Classification*

A low-dispersion spectrum of J205601, covering the wavelength region 3800 – 6000 Å, is shown in Figure 2. Through a comparison with MK spectral standards (Gray & Corbally 2009), we find that J205601 is an M4 red giant based on the strength of the observed TiO bands as well as the distinct features at 4626 and 4667 Å. In order to determine luminosity class, we looked at the strength of the MgH band near 4770, which is prominent in main sequence M stars. Using this, as well as direct comparisons between all M4 luminosity classes, we conclude J205601 to be a M-giant, specifically an M4 III.

Our measured $V = 11.60 \pm 0.03$ and $B = 13.26 \pm 0.03$ values for J205601 are consistent with Tycho-2 catalog values (Høg et al. 2000) of $V = 11.57 \pm 0.12$ and $B = 13.08 \pm 0.30$ (see Table 2). After correcting the observed $B - V$ for extinction to the Cygnus Loop of $E(B - V) = 0.08$ (Parker 1967; Raymond et al. 1981; Fesen et al. 1982), the star's $B - V$ of +1.58 is in line with $\simeq +1.62$ expected for an M4 III star (Cox 2000).

However, a range of $B - V$ values spanning 1.40 – 1.65 have been observed for M4 III stars (Pickles 1998) meaning there could be some extra visual extinction possibly due to dust in the star's surrounding nebulosity. An $E(B - V) > 0.08$ is also suggested by the fact that while its J-H and H-K values of 0.95 and 0.30 are close to tabulated values of M4 III stars (5.10; Bessell & Brett 1988;

Ducati et al. 2001), its V-K value of 5.74 is some 0.6 mag larger than expected possibly indicating an $E(B - V)$ closer to 0.20 mag.

3.1.2. *The Surrounding Bow-Shaped Nebulosity*

Figure 3 shows the location of J205601 in context within the Cygnus Loop's bright eastern nebula, NGC 6992. The left panel is an enlargement of the red DSS2 image centred several arcminutes west of the bright nebula, NGC 6992. This image reveals the presence of faint emission around J205601 roughly two arcminutes in size.

The nebula around J205601 is more apparent in the right panel which is a reproduction of Daniel Lopez's INT composite Hα + broadband filter image. In this image, the J205601 nebulosity appears highly filamentary, centred on and brightest to the west of J205601, and exhibiting a strong eastward curvature suggesting a bow shock morphology.

A deeper Hα image of the J205601 nebula is shown in Figure 4. Although lying at a significant distance west of NGC 6992, this image reveals faint emission extend eastward from the J205601 nebulosity over to the trailing edge of NGC 6992. The faint intervening emission is both diffuse and filamentary in places and, along with the lack of any detectable Hα emission west or south of J205601, suggests a physical connection between the J205601 nebula with NGC 6992, thus implying that they lie at the same approximate distance.
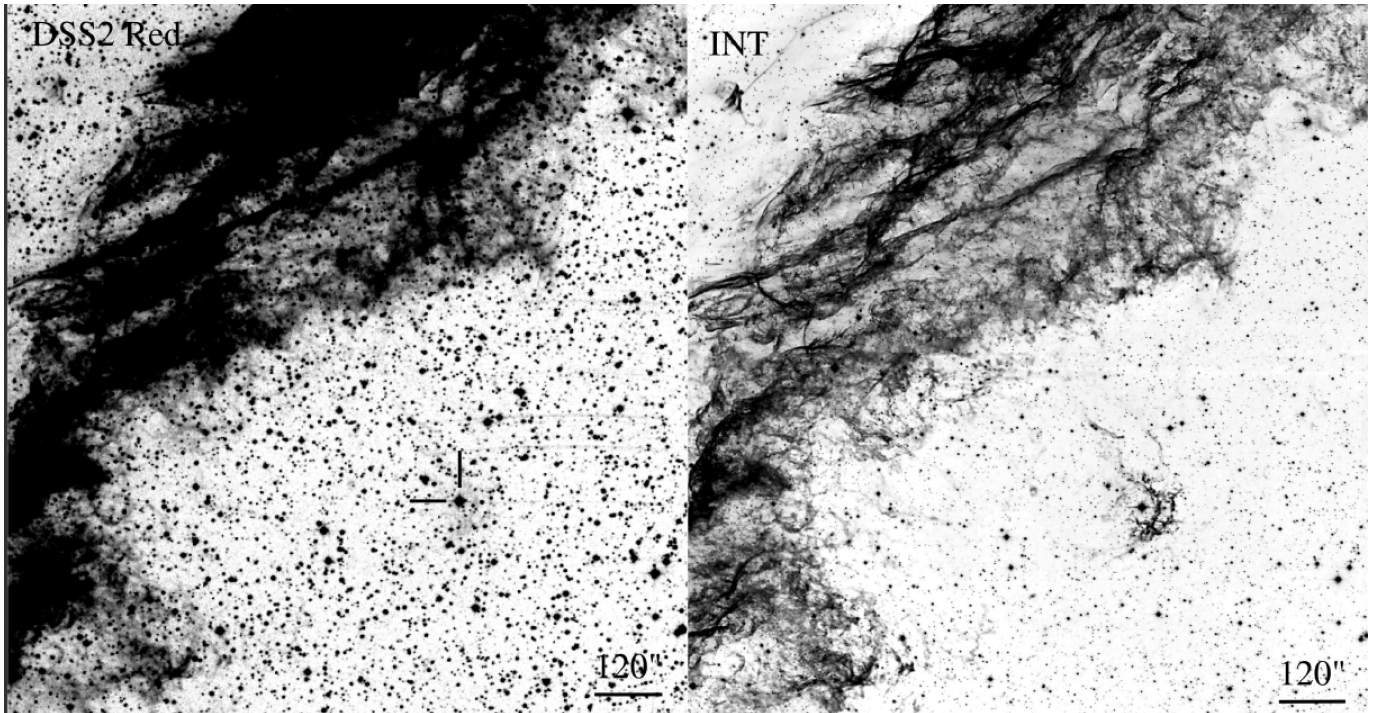
Fig. 3.— Left panel: Enlargement of the DSS2 red image of the south-central portion of NGC 6992 with the star J205601+313130 marked. Faint emission is seen around the star, mainly to the west. Right Panel: Same region imaged by Daniel Lopez using the Isaac Newton Telescope (INT) and a combination of broad filter and narrow Hα images which highlights the optical nebulosity around the star.

TABLE 3
Observed Relative Fluxes in the M Star Nebula

Line/Ratio	Pos 1a	Pos 1b	Pos 1c	Pos 2a	Pos 2b	Pos 2c
[O I] 6300	11	25	37	12	16	10
Hα 6563	100	100	100	100	100	100
[N II] 6583	80	98	84	92	95	96
[S II] 6716	56	54	50	47	43	39
[S II] 6731	52	48	42	45	42	38
[S II]/Hα	1.08	1.02	0.92	0.89	0.85	0.77
[S II] 6716/6731	1.08	1.12	1.20	1.04	1.02	1.03
ρ (cm^{-3})	430	360	250	510	560	540
Hα flux[a]	1.9	3.2	1.0	2.1	4.1	3.4

[a] Flux units: 10^{-15} erg s^{-1} cm^{-2}.

The J205601 nebula exhibits strong [S II] line emission relative to Hα, like that observed in supernova remnants and the majority of Cygnus Loop filaments (Fesen et al. 1982). This can be seen in Figure 5 which shows the J205601 nebulosity in the emission lines of Hα, [S II] 6716, 6716 Å, and [O III] 5007 Å.

In the Hα and [S II] images, the nebula appears to consist of two broken concentric rings of filaments centred on J205601. The filaments open to the north and south of the star and exhibit a morphology not unlike that of a wind-swept nebula. In contrast, little or no filament emission is seen in the [O III] image, where only faint, diffuse emission centred on the star is visible which may be, in part, reflections of J205601 in the narrow passband filter. Comparison of DSS1, DSS2, and our more recent images reveals significant eastward proper motion of the nebula's filaments somewhat smaller in magnitude to that seen in the neighboring NGC 6992 filaments.

Low-dispersion spectra of six locations in the J205601

nebula were taken using two E-W slits, as shown in Figure 6. The resulting spectra are shown in Figure 7 with observed relative fluxes are listed in Table 3.

These spectra clearly indicate that the nebula consists of shocked material. The relative strength of [S II]/Hα at all six locations is greater than the 0.4 criteria for identifying optical shocked material (Mathewson & Clarke 1972; Raymond 1979; Shull & McKee 1979; Dodorico et al. 1980; Dopita et al. 1984). Moreover, the absence of appreciable [O III] 4959, 5007 emission in the nebula (see Fig. 3) indicates a relatively low shock velocity. Shock models of interstellar shocks show that [O III] line emissions only become strong at velocities above 90 km s^{-1} (Shull & McKee 1979; Raymond 1979; Sutherland et al. 2003). A relatively low shock velocity in the 205601 nebula is in contrast with the majority of Cygnus Loop filaments, possibly the results of greater electron densities.

In fact, estimated electron densities in the J205601 nebula, based on the density sensitive [S II] 6716/6731
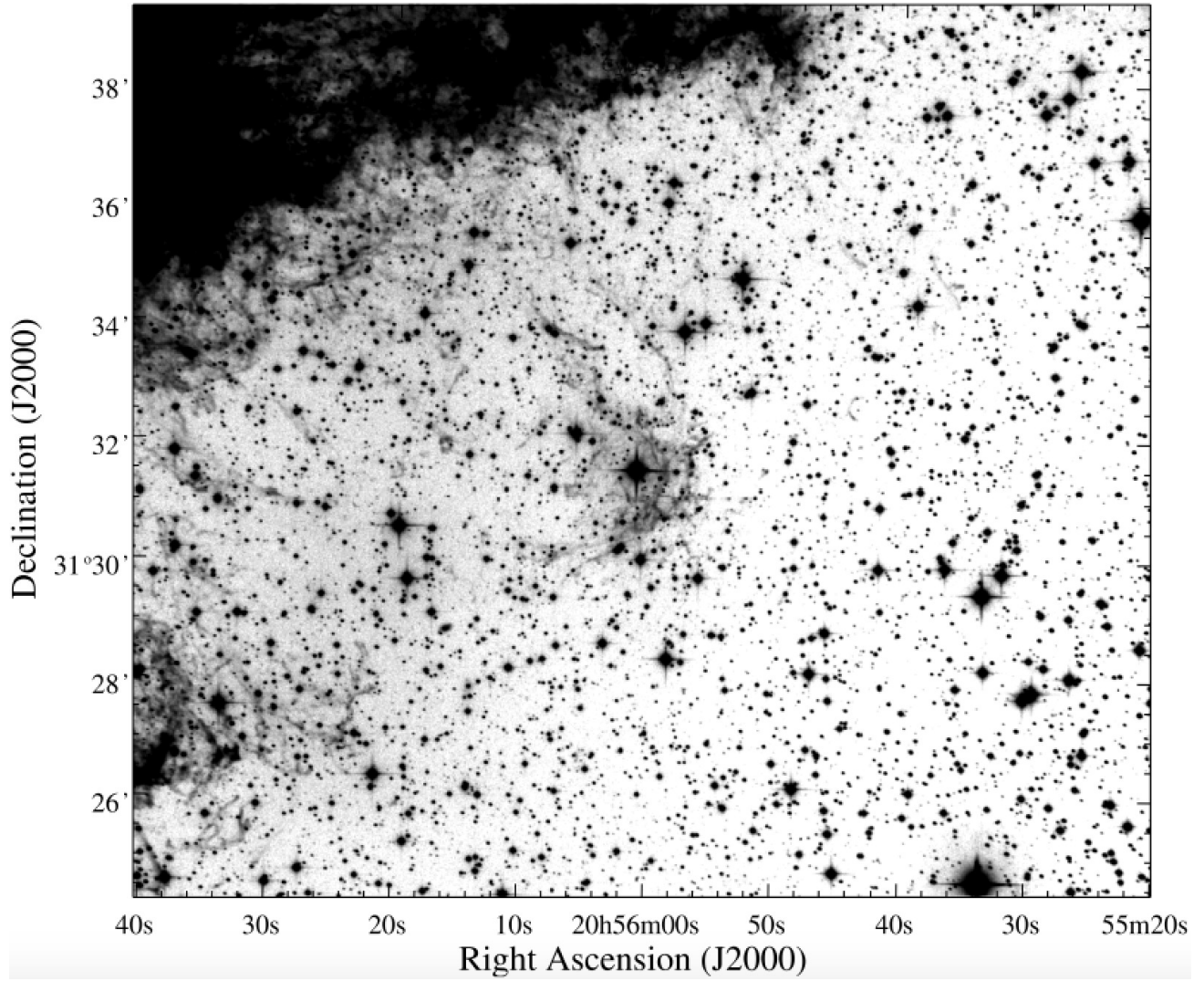
FIG. 4.— Hα image of the nebulosity around J205601+313130. Note the diffuse emission seen to the east of J205601 which appears to extend, broaden and merge in with the western edge of the Cygnus Loop's bright nebula NGC 6992. North is up, East to the left.
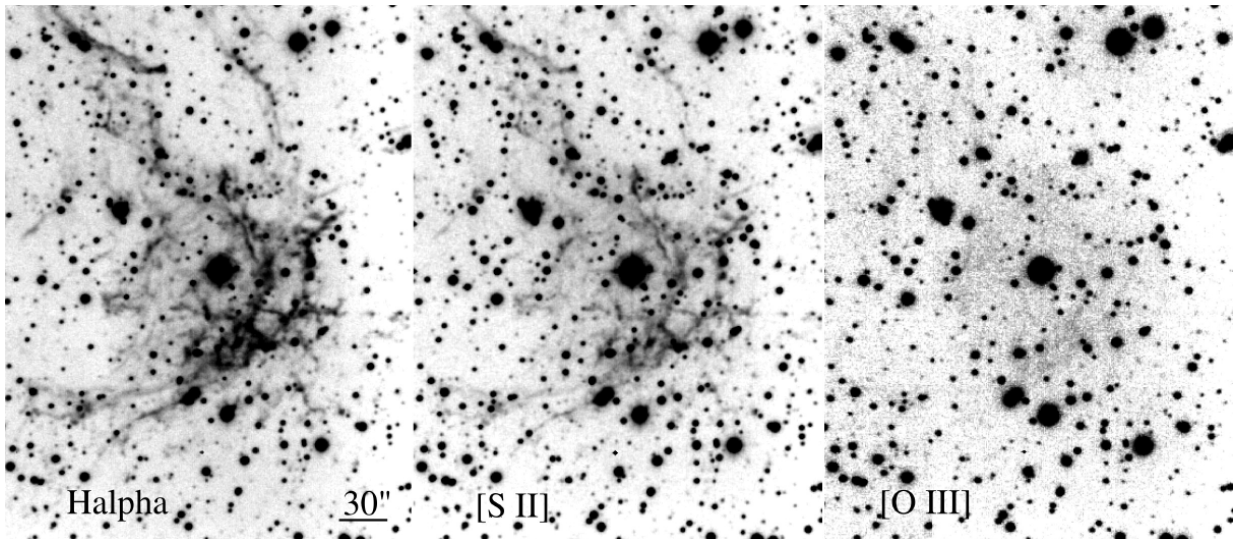

FIG. 5.— Images of the J205601 nebulosity taken in the light of Hα, [S II] λλ 6716,6731, and [O III] λ5007. North is up, East to the left.
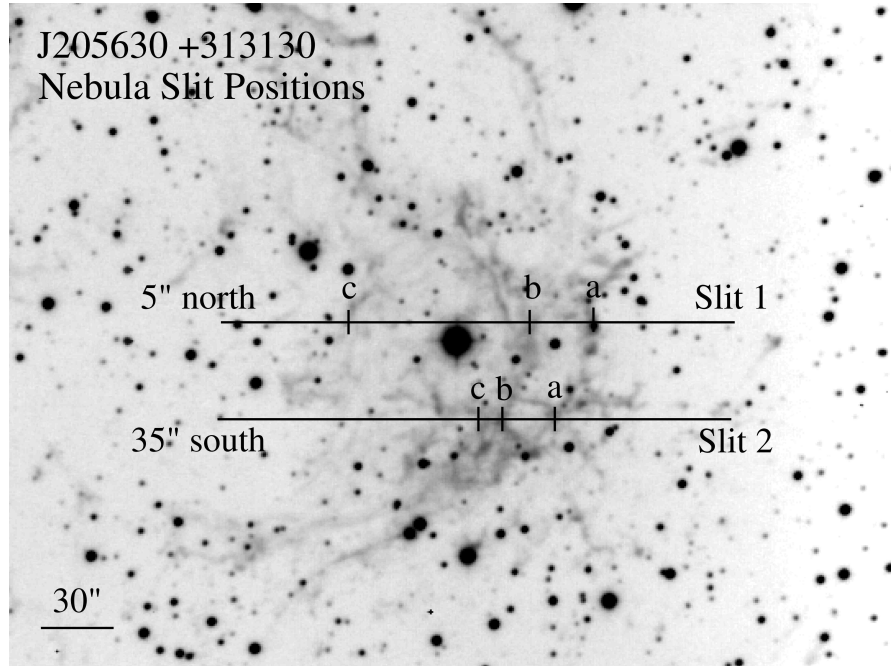
FIG. 6.— Slit positions in the nebulosity above and below J205601+313130 where low-dispersion red spectra were obtained (see Fig. 7). North is up, East to the left.
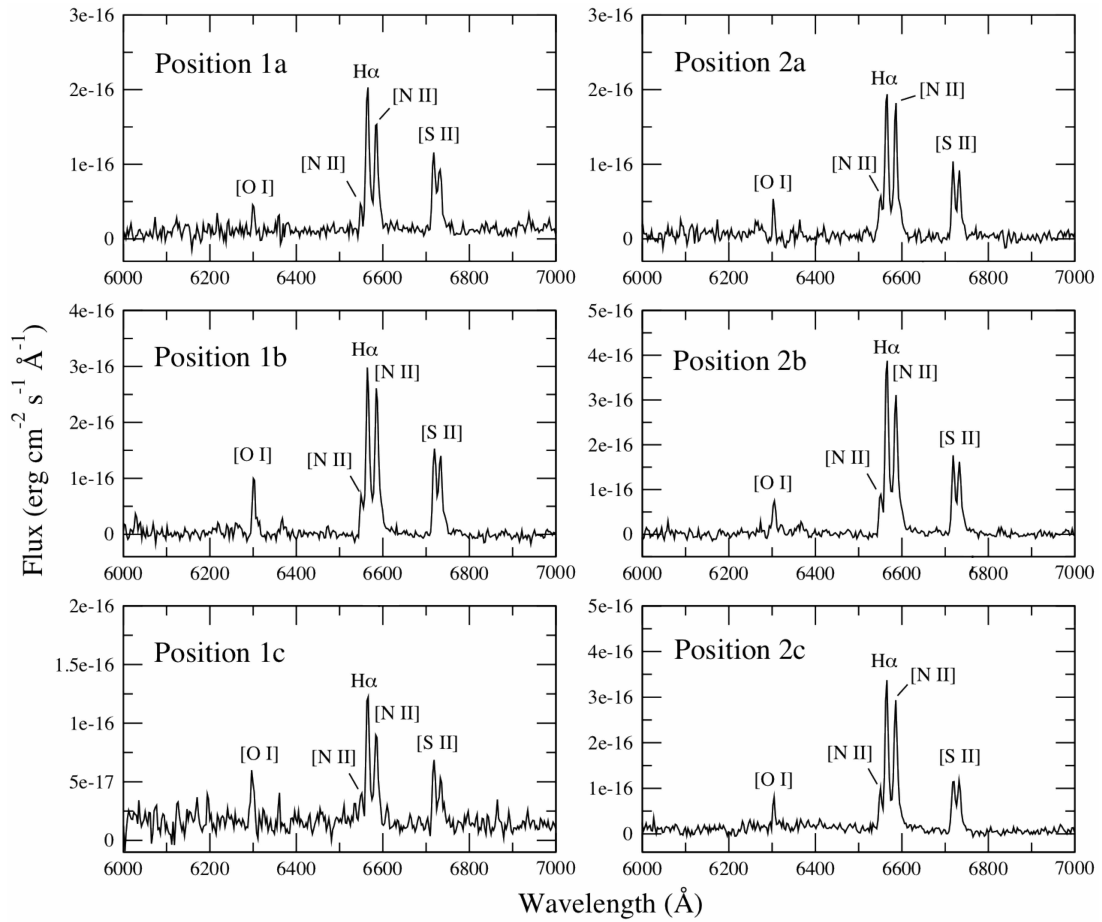

FIG. 7.— Spectra of six positions in the nebulosity around J205601 along slits Position 1 and 2 (see Fig. 6).

ratio, appears significantly higher than that seen generally in the Cygnus Loop's filaments. In a study of several of the remnant's brighter filaments, Fesen et al. (1982) found [S II] 6716/6731 values from 1.30 to 1.45, with the majority at or close to the low density of 1.43 (Osterbrock & Ferland 2006) indicating electron densities ≤ 100 cm^{-3} assuming an electron temperature of 10^4 K. Similar [S II] 6716/6731 lines above 1.30 were also found in an isolated ISM cloud in the SW region of the Cygnus Loop (Patnaude et al. 2002).

In contrast, the observed [S II] 6716/6731 line ratio for the six regions in the J205601 nebula show ratios from 1.02 to 1.20 indicating electron densities of roughly 250 - 550 cm^{-3} (Table 3). Although [S II] 6716/6731 line ratios around 1.2 were reported by Fesen & Hurford (1996) for two Cygnus Loop filaments, it appears that electron densities in the J205601 nebula are much higher than the majority of filaments in the Cygnus Loop remnant.

3.2. *BD+31 4224: A B7 Star in a Crescent Nebula*

A wide-angle Hα image of the northwestern limb of the Cygnus Loop is shown in Figure 8. This image is shown to highlight disturbances in the remnant's forward shock front along the remnant's northernmost boundary. One shock front disturbance can be seen associated with a small interstellar cloud, visible just left of image centre, and another shock front disturbance farther to the west near the star BD+31 4224.

It was not the presence of either disturbance in the remnant's northern shock front that first drew our attention to BD+31 4224. Rather, the star's location relative to a small crescent-shaped nebula (see below) that is only weakly visible on the red DSS2 image that led to an investigation into the nebula's nature and subsequently to this star.

3.2.1. *Stellar Classification*

A low-dispersion spectrum of BD+31 4224 covering the wavelength region 3800 – 6000 Å indicates it is a late B type star for which we have determined a spectral type of B7. As done an aid in spectral classification, we flattened its spectrum and the normalized flux plot of its spectrum is shown in Figure 9. This figure shows the important lines used in determining the spectral type, namely Si II 4128, 4130 Å, He I 4144,4471 Å, and Mg II 4481 Å. He I 4471/Mg II 4481 serves as a ratio to indicate late spectral types.

The classification of B7 is mainly on the basis of the comparison of He I 4471 Å with Mg II 4481 Å, and the weakness of the He I 4144 which fades in late B stars (Gray & Corbally 2009). Although the Si II 4128, 4130 Å features are somewhat obscured by the wide Hδ at 4102 Å, it appears that the Si 4128, 4130 Å lines are stronger than He I 4144 Å, firmly identifying it as B7.

Because of the factors listed above and the fact that it exhibits a spectrum virtually identical to the primary B7 V standard star standard HR 1029 (= HD 21071) (Keenan 1985; Garcia 1989; Garrison & Gray 1994; Gray & Corbally 2009), a spectral classification of B7 V appears secure. In addition, the star's observed extinction corrected $B - V$ value of -0.12 is consistent with standard B7 V $B-V$ values of -0.12 to -0.13 (Pickles 1998; Cox 2000; Mamajek 2017).

Although a dwarf luminosity classification (V) is indicated based on the broadness of its hydrogen lines, we could not completely rule out a possible subgiant IV classification based upon the weakness of O II 4070 and 4416 Å lines due to our spectrum's relative low S/N.

Our photometric observations of this star agree with values from the Tycho-2 catalog (Høg et al. 2000). Specifically, we measured V = 9.59 ± 0.02 and B = 9.55 ± 0.03 which are close to the listed Tycho-2 values of V = 9.58 and B = 9.53 (see Table 2).

3.2.2. *Nebulosities Near BD+31 4224*

The faint nebulosities near and around BD+31 4224 are better seen in Figure 10. A relatively deep Hα image is presented in the top panel, with enlargements of an area immediately around BD+31 4224 shown in the bottom panels. As seen in these images, Hα emission filaments associated with the Cygnus Loop's forward shock exhibit a strong distortion at its northernmost boundary near BD+31 4224. Specifically, a "blow-out" of the remnant's shock front can be seen along with several highly curved Hα filaments with BD+31 4224 appearing symmetrically placed relative to these emission features.

On smaller scales, BD+31 4224 lies centred within a bow-shaped emission arc. Figure 11 shows images of this emission arc taken in Hα, [S II] 6716, 6731 Å and [O III] 5007 Å. Noticeably stronger Hα and [S II] emission is seen at the northern and southern tips of the bow-shaped nebula, whereas [O III] is strongest in its middle and closest to BD+31 4224.

Emission can be seen to extend about 2 arcminutes to the northeast of BD+31 4224, especially prominent in the [O III] image, and near a noticeable but fainter star compared to BD+31 4224 (m_V = 12.0; TYC 2691-1550-1). A spectrum shows it to be a K dwarf and it has a Tycho-GAIA determined parallax measurement of 7.70 ± 0.29 (Gaia Collaboration et al. 2016). Its optical spectrum, observed magnitude, and measured parallax indicates it lies at ~ 130 pc and is thus unrelated to the Cygnus Loop and the observed emission filaments.

Optical spectra were obtained at three positions in the bright nebula arc west of BD+31 4224, plus one position in a filament of similar brightness located some $150''$ northeast of BD+31 4224 (see Fig. 12). The resulting spectra of these four regions are shown in Figure 13 with observed relative line strengths listed in Table 3.

The observed strength of the [S II] 6716, 6731 Å lines relative to that of Hα clearly indicate that all four regions represent shock emission. The spectrum of the filament off to the NE of BD+31 4224 is not markedly different from that seen in the bow-shaped arc nebula centred on BD+31 4224. However, unlike that seen in the J205601 nebula where the density sensitive [S II] lines indicate electron densities above 250 cm^{-3}, the shocked nebulosities around BD+31 4224 are much lower $\lesssim 100$ cm^{-3} near the low density limit of 1.43 (Osterbrock & Ferland 2006).

The strength of the [N II] 6548, 6583 Å lines relative to that of Hα are relatively strong but not unusual for SNRs and in particular Cygnus Loop filaments (Fesen et al. 1982; Fesen & Hurford 1996). The same holds true for the [O III] lines. However, there is a significant difference in the [O III] strength at either end of the bow-shaped
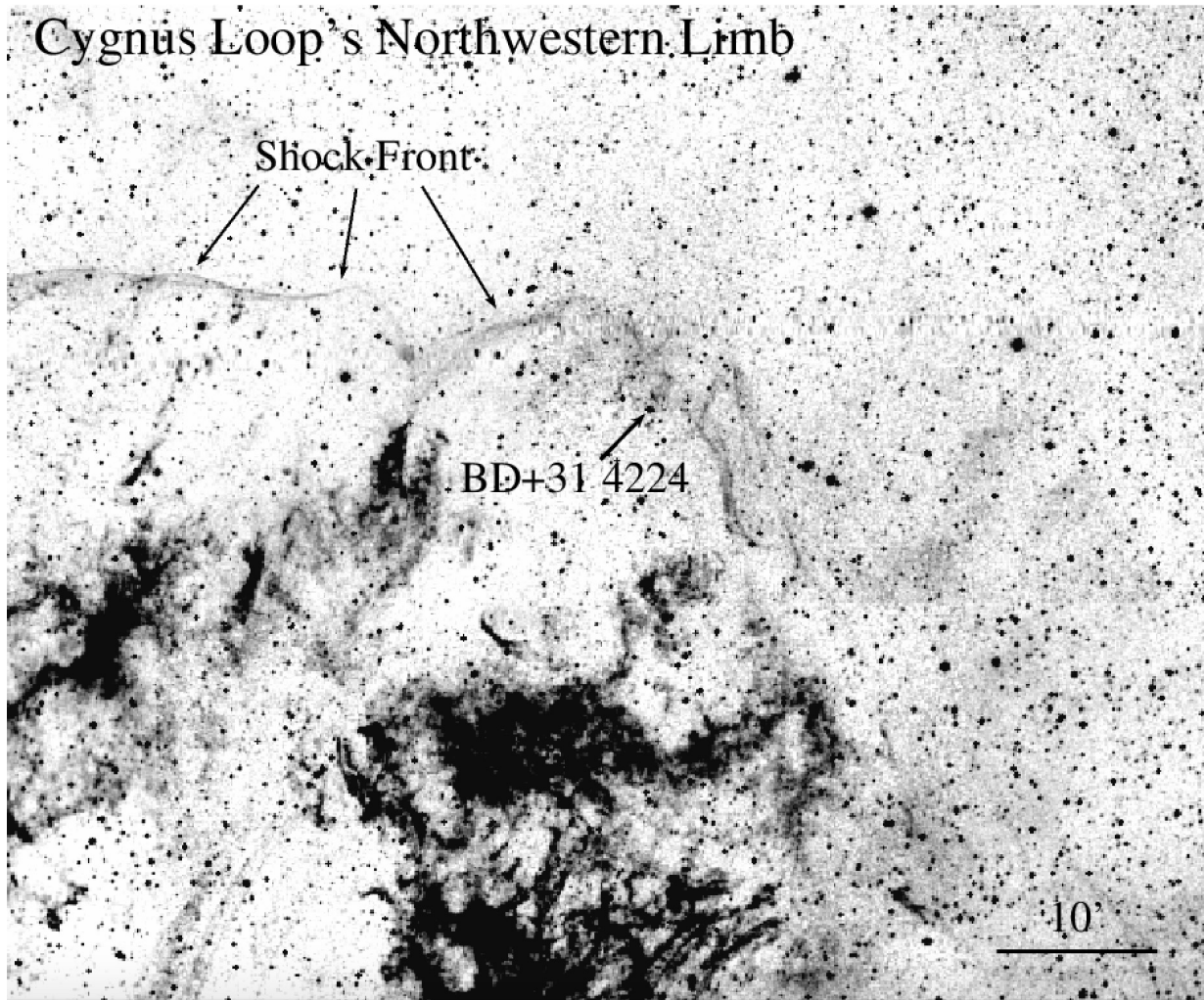
FIG. 8.— Wide field Schmidt Hα image of the northwestern limb of the Cygnus Loop showing disturbances of the remnant's forward shock front, one in the region near BD+31 4224. North is up, East to the left.

nebula (Pos 1a and Pos 3) versus Pos 1b, closer to the B star BD+31 4224. This is consistent with the narrow passband images shown in Figure 11.

The location of BD+31 4224, a B7 star which is expected to have relatively high-velocity stellar winds, at the centre of a small bow-shaped nebula, brightest in [O III] closest to the star, and symmetrically placed in relation to a series of highly curved filaments and situated near a shock front blow-out along the remnant's northern shock boundary together comprise strong evidence for a physical connection of the star's stellar winds and the Cygnus Loop's shock wave. In this scenario, the B7 star's winds interacted with the remnant's shock front creating both the observed bow-shock nebula centred on the star and the distorted filaments and shock front break-out in this northwestern limb region.

4. DISCUSSION

Underlying every quantitative discussion of the Cygnus Loop is uncertainty of its distance. As shown in Table 1, prior distance estimates have ranged from less than 0.4 to nearly 2.0 kpc. Because of the remnant's prominent place in the study of evolved Galactic SNRs at all wavelengths, it is important to determine its distance to a greater

TABLE 4
RELATIVE FLUXES IN NEBULA NEAR BD+31 4224

Line/Ratio	Pos 1a	Pos 1b	Pos 2	Pos 3
[O III] 4363	...	25	–	...
Hβ 4861	100	100	100	100
[O III] 5007	90	2020	850	475
Hα 6563	315	300	285	315
[N II] 6583	265	280	355	305
[S II] 6716	210	225	260	175
[S II] 6731	175	(142)	175	137
[S II]/Hα	1.23	1.23	1.52	1.00
[S II] 6716/6731	1.20	(1.6)	1.48	1.28
ρ (cm^{-3})	250	<100	<100	150
Hα flux[a]	3.5	1.2	5.8	1.4

[a] Flux units: 10^{-15} erg s^{-1} cm^{-2}.

degree of certainty. Below, we first review some of the previous distance measurements and then describe how the two stars discussed above may help resolve this issue.

4.1. Previous Distance Estimates to the Cygnus Loop

Until the mid-1970's, the most widely adopted value for the Cygnus Loop's distance was from a kinematic investigation by Minkowski (1958). This approach has
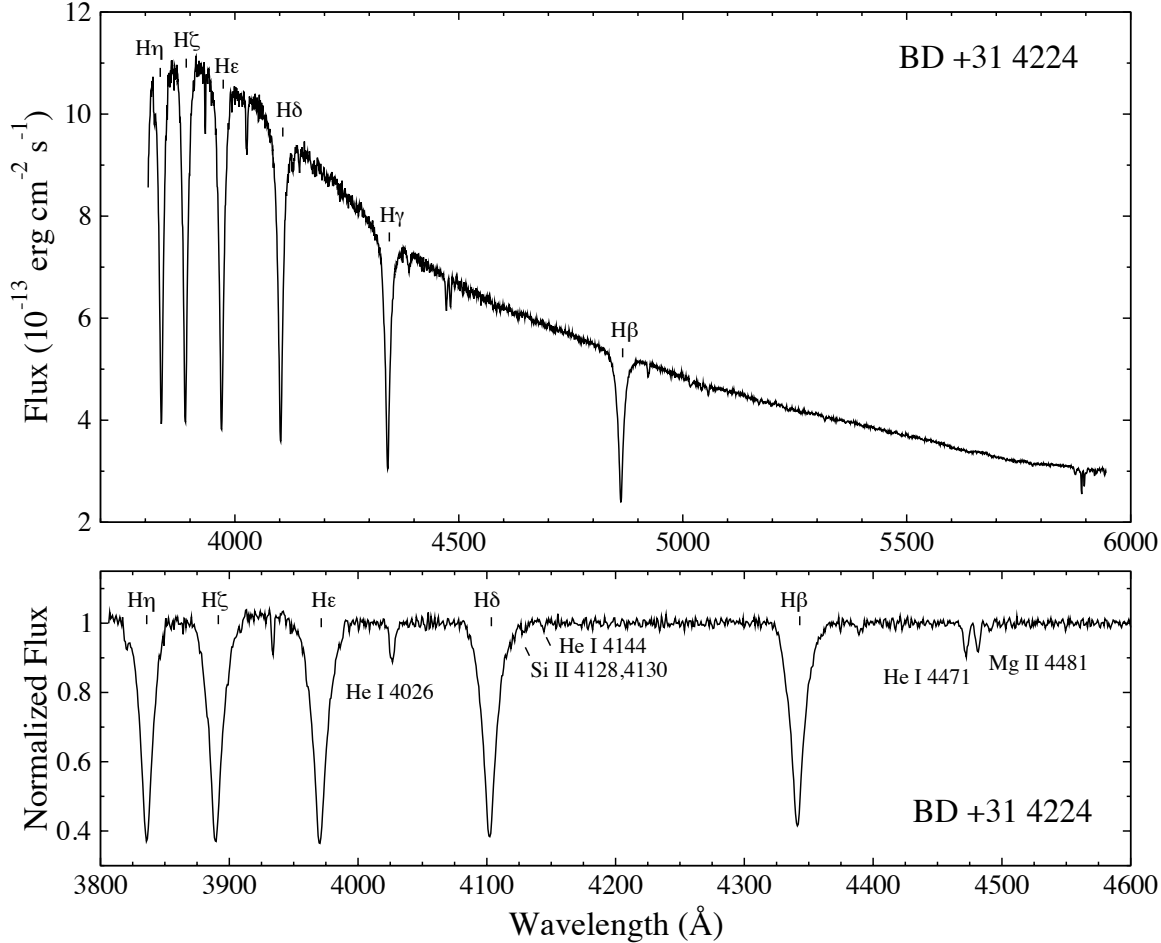
FIG. 9.— Observed (top) and normalized (bottom) spectrum of BD+31 4224.

the inherent uncertainty of connecting proper motions seen in one set of filaments with the radial velocities or inferred shock velocity found for some other filaments.

Consequently, Minkowski's Cygnus Loop distance estimate began to be questioned. McKee & Cowie (1975) suggested 770 pc might be an underestimate while Kirshner (1976) thought it was much too large. Subsequently, a number of distances estimates were proposed usually relying on combining proper motion with shock velocity measurements or estimates (see Table 1).

Blair et al. (1999) compared the locations of non-radiative filaments along the remnants northeastern limb on a digitized version of the 1953 DSS1 red plate of the Cygnus Loop and on a 1997 Wide Field Planetary Camera2 (WFPC2) *Hubble Space Telescope* Hα image to deduce a value of 440^{+130}_{-100} pc. Later measurements of these same filaments based solely on *HST* images taken 4 years apart resulted in a revised value of 540^{+130}_{-80} pc (Blair et al. 2005).

An upper limit to the distance to the Cygnus Loop was later proposed based on optical and far UV observations of sdOB star lying in the direction to Cygnus Loop's eastern NGC 6992 nebulosity which showed broad O VI λ 1032 line absorption indicating it lies behind the remnant (Blair et al. 2009). Model fits to this star's optical and

UV spectra yielded a $T_{eff} = 35,500 \pm 1000$ K and a distance of 576±61 pc, a value consistent with the earlier remnant estimate by Blair et al. (2005).

More recently, Medina et al. (2014) obtained high-resolution Echelle spectra of faint Balmer-dominated Hα filaments along the remnant's northeastern limb to estimate shock velocities of around 400 km s^{-1} from the broad Hα emission component. They then combined this value with proper motions measured by Salvesen et al. (2009) over a 39 year time span to deduce a distance to the Cygnus Loop of ∼890 pc (786 – 1176 pc). A follow-up analysis of thermal equilibrium in a collisionless shock affecting the broad Hα component led to a reduction of the derived shock velocity down from 400 to ∼360 km s^{-1}, which thereby decreased the Cygnus Loop's estimated distance from 890 to 800 pc (Raymond et al. 2015).

While higher shock velocity estimates associated with the remnant's faint, outer Balmer-dominated Hα filaments may explain the relatively low earlier Cygnus Loop distance estimates around 500 and 600 pc, the detection of O VI λ 1032 line absorption in an sdOB star found by Blair et al. (2009) along the remnant's eastern limb at an estimated distance of just ∼ 575 pc is puzzling.

Their spectral analysis of both UV and optical spectra of this star by Blair et al. (2009) was thorough and

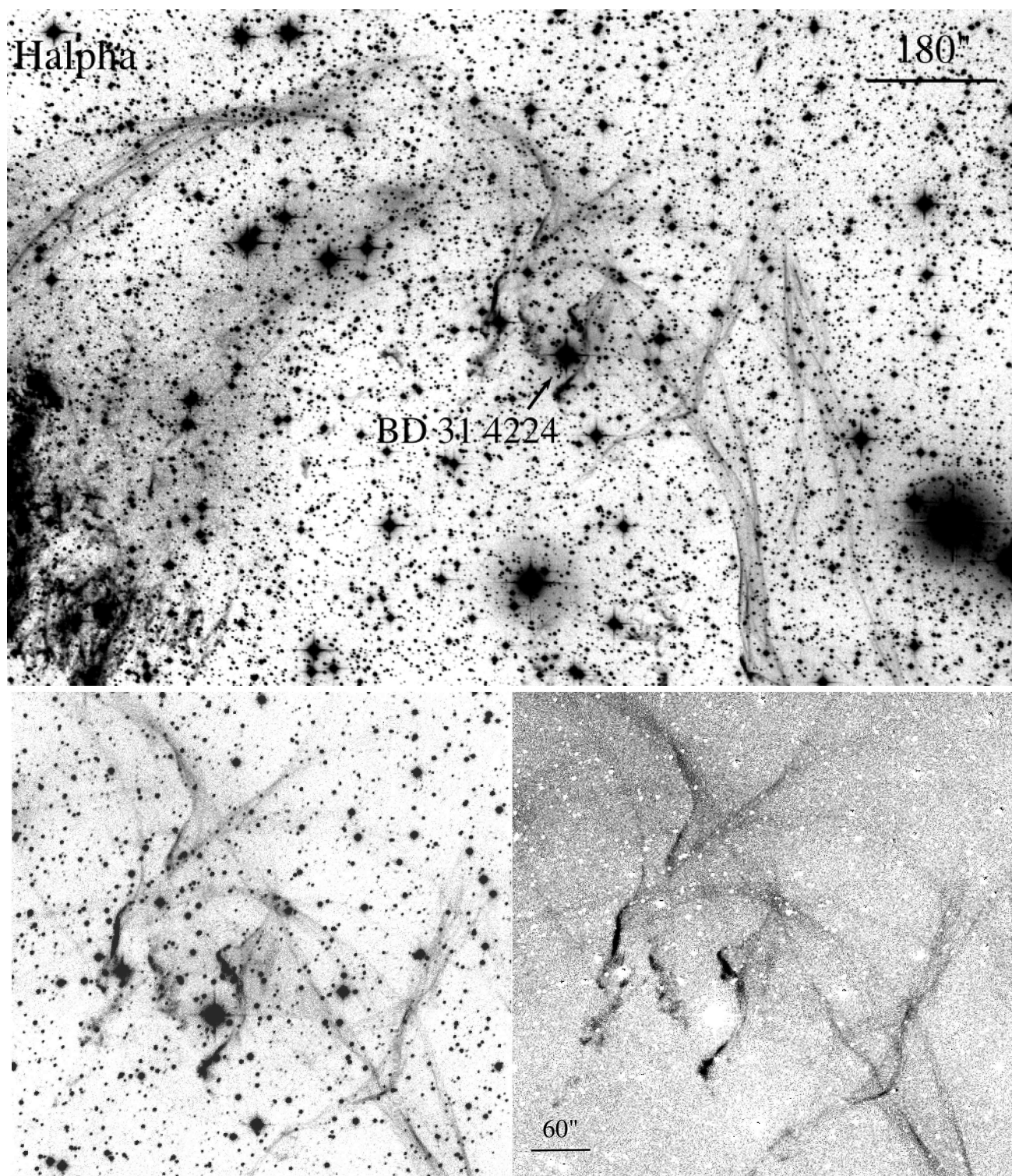FIG. 10.— Top Panel: Deep Hα image of the emission structure along the Cygnus Loop's northeastern limb and centred on the B star BD+31 4224. North is up, East to the left. Bottom Panels: Enlargement of the Hα image with stars (left) and with stars partially removed (right) to better reveal the filaments and nebulosity around BD+31 4224.
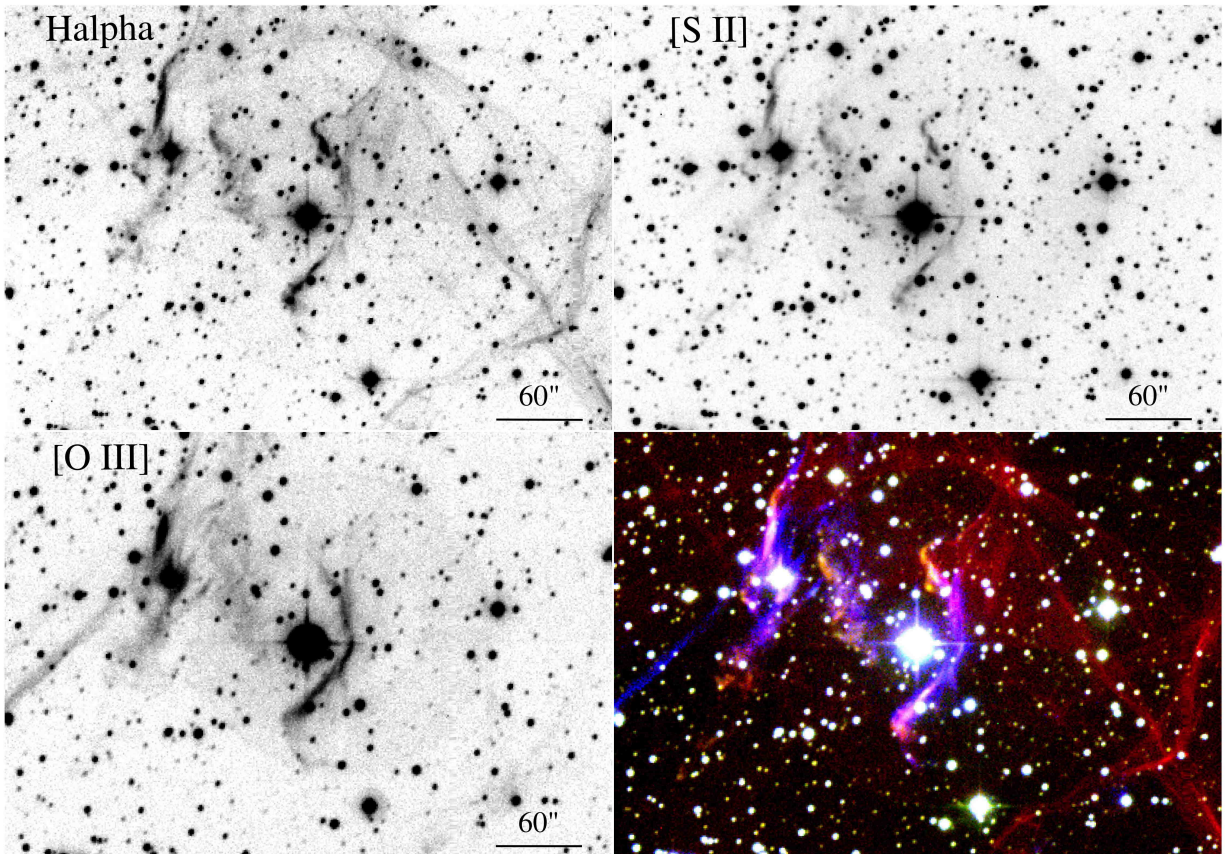
FIG. 11.— Hα, [S II] 6716,6731 and [O III] 5007 images of the emission structure around the B star BD+31 4224 along with a color composite (Hα red, [S II] green, & [O III] blue). Note the similarity of the Hα and [S II] images and the contrast with that of the [O III] image especially the centre of the emission arc nearest the B star. North is up, East to the left.
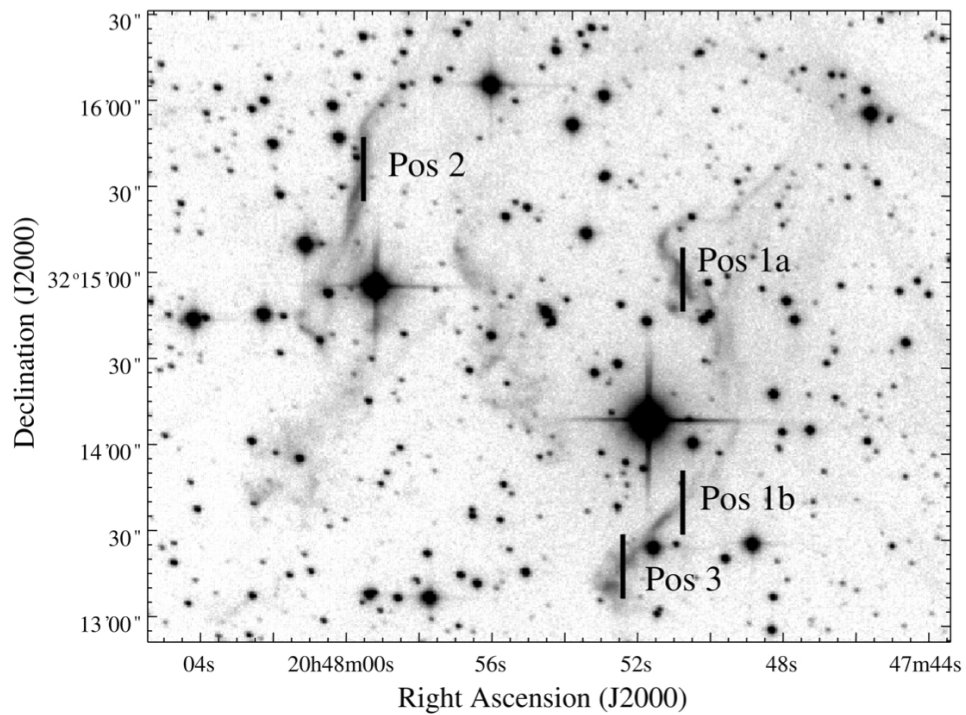

FIG. 12.— Slit positions in the nebulosity around the B star BD+31 4224 where low-dispersion red spectra were obtained (see Fig. 12). North is up, East to the left.
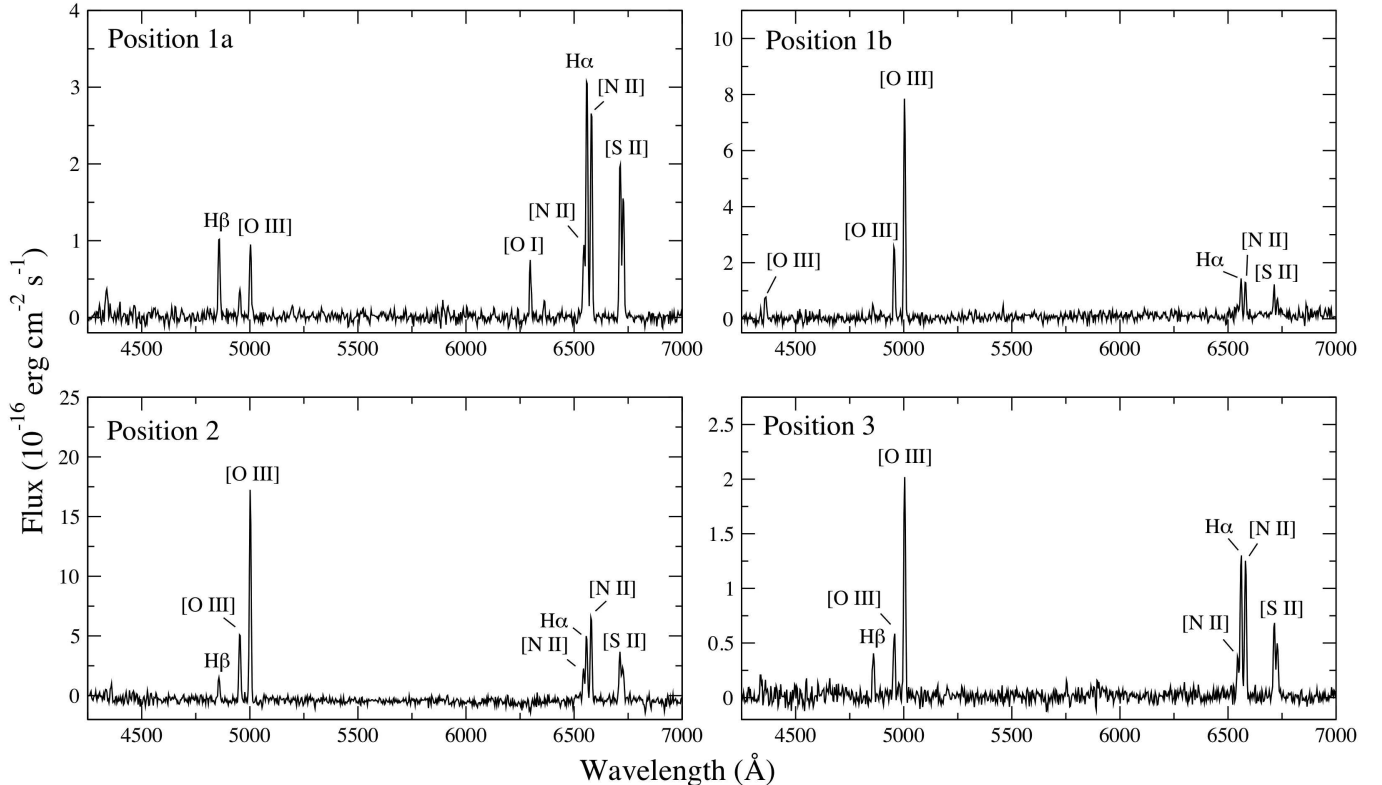
FIG. 13.— Spectra of filaments near BD+31 4224. See Figure 12 for slit positions.

robust, implying an $M_V = +5.23$ for this $m_V = 14.12$ sdOB star. However, some hot sdOB stars with $T_{eff} \approx$ 35,000 K similar to this sdOB star exhibit $M_V = +2.5$ to $+4.5$ (de Boer et al. 1997), which is much brighter that than estimated by Blair et al. (2009). This raises at least the possibility of a larger distance to this star than the analysis of its spectral properties might indicate.

4.2. *Problems with Distances Less Than 650 pc*

Salvesen et al. (2009) investigated the ratio of cosmic ray pressure to gas pressure in several regions in the remnant. They constrained the shock speeds of 18 non-radiative filaments through proper motion measurements seen along the remnant's northeastern limb from Digital Sky Survey I and II images and adopting a distance of 637 pc, the maximum allowed by the sdOB star observation of Blair et al. (2009). Salvesen et al. (2009) then deduced post-shock electron temperatures from spectral fits to *ROSAT* PSPC observations along the perimeter of the remnant and found that in most cases the this ratio was either low or formally negative even when adopting the maximum distance estimated of 640 pc by Blair et al. (2009).

Salvesen et al. (2009) concluded the cause for the many implausible negative ratios calculated was the significant uncertainty in the postshock temperature measurements. However, they also wondered if the Cygnus Loop's distance might be larger than 650 pc, but thought it was unlikely to be as large as the ~ 1 kpc that would be needed to make all the upper limits to P_{CR}/P_G positive.

Interestingly, it has been long known that models of the Cygnus Loop remnant assuming distances less than 1 kpc result in an energetically weak SN explosion. Based on the framework of the Sedov model, the estimated remnant's energy using Minkowski's 770 pc distance estimate is just $E_0 = 3 - 7 \times 10^{50}$ $(d_{pc}/770)^{5/2}$ erg, considerably less than the canonical SN explosion energy of $1 - 2 \times 10^{51}$ erg (Rappaport et al. 1974; Falle & Garlick 1982; Ballet et al. 1984; Miyata & Tsunemi 1999) with smaller distances of around $0.5 - 0.6$ kpc implying an even weaker SN event.

The problem of an energetically weak SN for the Cygnus Loop was highlighted in a recent modeling study by Preite Martinez (2011). He examined the global parameters of the remnant assuming a low-density cavity model and using a time-dependent spherically-symmetric hydrodynamical code and found that a distance of 540 pc resulted in an estimated supernova explosion energy of just $6 - 8 \times 10^{49}$ erg. A similar analysis undertaken by Fang et al. (2017) who estimated a somewhat higher energy of 2×10^{50} erg. But both estimates fall well short of a value near 10^{51} erg.

Preite Martinez (2011) concluded that if the Cygnus Loop were at a distance of ≈ 0.6 kpc it must have been an unusually weak core-collapse event, perhaps "the weakest known core-collapse SN in the Galaxy". He further noted that much greater distances, ~ 1.25 kpc, would be needed to recover a "standard" SN energy $E_0 \sim 1 \times 10^{51}$ erg but viewed this unlikely as it was well outside quoted uncertainties of the Blair et al. (2009) estimate.

4.3. *A Distance Based on Stellar Distances*

The results of our imaging and spectroscopic investigations of nebulosities seen around the M4 III star J205601 and the B7 V-IV star BD+31 4224 presented in §3 sug-

gest they are circumstellar features resulting from interaction of stellar mass loss material with the remnant's expanding shock front. If true, this means that both stars lie inside the remnant and thus can be used to estimate the remnant's distance using spectroscopic parallax derived distances.

We can estimate the distances to these two stars using the familiar distance modulus equation

$$log\ d_{pc} = (m_V - M_V + 5 - A_V)/5 \qquad (1)$$

where $A_V = R(V) \times E(B-V)$ is the extinction. Using the color-excess estimate for the Cygnus Loop, $E(B-V) = 0.08$ (Parker 1967; Raymond et al. 1981; Fesen et al. 1982) and $R(V) = 3.1$, then $A_V = 0.25$.

Absolute visual magnitude values red giants can span a wide range. Gray & Corbally (2009) list average M_V values for M4 III stars between -1.1 and -2.2 corresponding to luminosity classes IIIa and IIIb consistent with globular cluster measurements, while general reference sources cite values for an M4 III star, like J205601, to be -0.4 to -0.6 (Lang 1992; Cox 2000).

However, *Hipparcos* measurements of field stars indicate an even broader range of M_V values for red giants. For an M4 III with a B-V value $\sim$1.6, the observed M_V spans roughly from -2.0 to +1.5 (Kovalevsky 1998). Using measurements just for the roughly 49,000 stars with *Hipparcos* parallax measurement accuracy better than 20%, one finds the range of M_V is -2.0 to $+1.0$ (ESA 1997). Adopting these values, we estimate the distance to J205601, and hence to the Cygnus Loop, to be between 1.2 and 4.6 kpc. If the $E(B-V)$ to J205601 is closer to $\sim$0.20 rather than 0.08 due to extra extinction arising from the surrounding nebulosity, then this distance range decreases to 1.0 and 3.9 kpc.

Distances to the Cygnus Loop much greater than $\sim$2 kpc are highly unlikely for several reasons. These include implied remnant size and age at such distances given the remnant's observed X-ray and optical shock properties, along with filament proper motion relative to measured filament radial velocities.

However, the fact that J205601 might well lie at distances much greater than 2 kpc raises the question of whether or not it actually lies, in fact, inside the Cygnus Loop. After all, thousands of stars are projected within the remnant's boundaries. Thus one can not, *a piori*, discount the possibility that this red giant is simply a background star located far away and unrelated to both the Cygnus Loop and the nebulosity described above seen in its direction.

While it is almost certain that the nebulosity seen toward J205601 represents material shocked by the Cygnus Loop's shock front and thereby lies inside the remnant, a direct physical connection of this red giant with the nebulosity is not definitive. Our red spectrum of J205601 revealed no Hα emission that could strengthen the scenario of on-going mass loss supporting the formation of the observed surrounding nebula. There is also the requirement that J205601 be a relatively faint M4 red giant (although not the faintest) in order to lie at a distance less than 2 kpc.

However, the combination of J205601 being a red giant, a type of star known to undergo substantial mass loss, and it's location near the geometric centre of a small

bow-shaped nebula strongly suggests that J205601 lies physically inside, and is the source of, the observed nebula. The nebula's higher electron densities compared to almost all of Cygnus Loop' filaments, along with its unusual bow-shaped morphology also point to an unusual origin. Furthermore, it is unlikely to be just a small, isolated ISM cloud that has been shocked by passage of the remnant's shock front because it possesses quite a different morphology from that of other known small ISM clouds overrun, shocked, and accelerated by the Cygnus Loop's blast wave (Fesen et al. 1992; Patnaude et al. 2002).

Thus the preponderance of evidence indicates that the red giant J205601 likely lies within the Cygnus Loop and inside its surrounding nebula, therefore implying a distance to the remnant on the high side of the 0.4 – 2.0 kpc prior distance estimates (Table 1). On the other hand, for J205601 to be inside the remnant, distances less than 0.8 kpc are firmly excluded. That is because even if J205601's luminosity were that seen for the faintest observed M4 red giants (i.e., $M_V = +1.5$) and assuming an $E(B-V) = 0.2$, it's distance would be $\sim$ 0.8 kpc.

With an angular radius of $\sim$ 1 arcminute, the J205601 nebula is $\simeq 0.3 \times$(d/1.0 kpc) pc in size. Although some of its material could be red giant mass loss material off J205601, a significant fraction is likely swept-up ISM gas. Assuming an association with J205601 and an undecelerated red giant wind velocity of 10 km s^{-1}, the nebula's dimension suggest a mass loss time frame of $\lesssim$ 50,000 yr, with the nebula's double shell appearance suggesting the mass loss occurred in two major episodes.

Distance estimates to the B star BD+31 4224 are more restrictive. The most quoted absolute Johnson V magnitude for a B7 V star is -0.40 (Jaschek & Gomez 1998; Gray & Corbally 2009; Mamajek 2017). Adopting an apparent magnitude of 9.58 for BD+31 4224, a M_V value of -0.4 and an $A_V = 0.25$ mag consistent with its observed $E(B-V)$, translates to a distance of 880 pc.

However, a range of absolute Johnson magnitudes for B7 V stars have been cited in recent literature, with Mamajek (2017) listing M_V values from -0.11 to -0.67; e.g., Lang (1992) lists $M_V = -0.6$ while Wegner (2006) gives -0.63 based on *Hipparcos* parallaxes for 138 B7 V stars. Adopting M_V values of -0.1 to -0.67, estimated distances to BD+31 4224 range from 770 to 1000 pc.

Since we were not able to completely rule out a B7 IV classification, we have also calculated a maximum distance to BD+31 4224 if it were a B7 IV star. Using M_V values of -0.77 to -1.3 for B7 IV stars (Wegner 2006; Gray & Corbally 2009), we obtain distances of 1050 and 1330 pc. However, given that BD+31 4224's spectrum and colors match so well primary B7 V standards, we view smaller distances of 800 to 1000 pc as more likely.

In summary, the B7 V star BD+31 4224 suggests a Cygnus Loop distance around 0.8 to 1.0 kpc, while the M4 III star J205601 points to a distance of at least 1 kpc. The fact that there is little overlap in the estimated distances to two stars which we believe both lie inside the remnant, suggests that the remnant lies at a distance of $\sim$1 kpc and hence farther than many previous estimates. Based on distance estimates to these stars, but giving greater weight to smaller distance estimates arising from the B7 star, we conclude the Cygnus Loop lies at a dis-
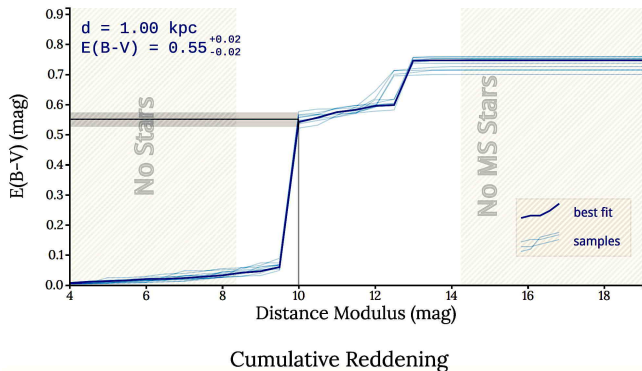
FIG. 14.— Pan-STARRS1 derived plot of cumulative dust reddening along the western limb of the Cygnus Loop at α[J2000] = 20^{h}45^{m}13^s, δ[J2000] = +30.5°. Made using website: https://argonaut.skymaps.info.

tance of 0.8 - 1.2 kpc.

4.4. A Distance Estimate Using Dust Reddening along the Cygnus Loop's Western Limb

We note that a distance to the Cygnus Loop $\simeq 1$ kpc is consistent with estimates for the distance to a large molecular cloud situated along with remnant's western limb and long viewed as likely being impacted by the remnant's shock front. Duncan (1923) described NGC 6960 as the "frontier between a region of many faint stars on the east and fewer on the west", with both Wolf (1923) and Oort (1946) noting that the remnant's bright western nebulosity lies at the precise border of a dark nebula to the west.

The presence of dust from this molecular cloud is obvious on images published by Ross (1931) who noted that NGC 6960 lies on the boundary of a very extensive dark nebula with striking differences in stellar density east and west of the nebula. Star density differences on either side of NGC 6960 is most apparent in wide-angle blue images of the remnant and these differences have been well studied by both Chamberlain (1953) and Bok & Warwick (1957).

CO maps of Scoville et al. (1977) show the presence of a large molecular cloud near the remnant's western emission (NGC 6960) with excellent correlation with the observed optical obscuration. Levenson et al. (1996) examined the optical and X-ray emission along the western limb of the Cygnus Loop and concluded the remnant was directly interacting with this cloud.

Figure 14 shows a plot of dust reddening with distance along the western limb of the Cygnus Loop based on a three-dimensional map presented in Green et al. (2015), which utilizes Pan-STARRS (Schlafly et al. 2014) and 2MASS (Skrutskie et al. 2006) photometry. This figure shows a sharp rise of extinction at 1 kpc, which then steadily increases from 1.0 out to 3.1 kpc, then rises again out to 4 kpc where E(B-V) reaches 0.75 mag. The sharp rise of extinction at 1 kpc is presumably due to the CO cloud the remnant appears to be physically encountering and we take this as additional supporting evidence for a distance to the Cygnus Loop of around 1 kpc.

The presence of some of the remnant's shock filaments some 25′ to 30′ farther to the west of the the Cygnus Loop's bright western nebula, NGC 6960, (see Fig. 4 in Fesen et al. 1992) suggests the remnant lies close to the near side of the molecular cloud. If correct, this then means that the remnant's distance is probably closer to 0.8 – 1.0 kpc than much larger values suggested by the M star.

5. CONCLUSIONS

The Cygnus Loop is among the brightest and best studied Galactic supernova remnants. Unfortunately, like many other Galactic remnants, its distance has not yet been determined to high accuracy.

Here we present optical images and spectra of two small nebulosities with projection locations within the Cygnus Loop supernova remnant which we suspect are the results of stellar wind material interacting with the remnant's expanding shock wave. We have identified one star within each of these two nebulae which we propose as the source of their respective surrounding nebula and use optical photometry and spectra to estimate their distances via spectroscopic parallax. We then use the resulting stellar distance estimates to then constrain the Cygnus Loop's distance.

We find that an M4 III star located near the centre of a shocked, bow-shaped nebula situated a few arcminutes west of the Cygnus Loop's bright eastern nebula NGC 6992 lies at an estimated distance of between 1.0 and 4.6 kpc. A B7 V star located along the remnant's northwestern limb and centred in an arc of shocked emission surrounded by a much larger region of curved and twisted filaments likely lies at a distance of between 0.8 and 1.0 kpc.

A Cygnus Loop distance of around 1 kpc would be consistent with the estimated distance to a molecular cloud situated along the remnant's western limb with which the remnant appears to be interacting. Thus, based on the assumption that these two stars lie inside the remnant, combined with the estimated distance to a molecular cloud situated along the remnant's western limb, we propose a distance to the Cygnus Loop of 1.0 ± 0.2 kpc. A distance of 1.0 kpc implies a physical size for the remnant of $\approx 50 \times 60$ pc.

A distance around 1 kpc would help to resolve the issue of deduced postshock cosmic ray to gas pressure ratios being near zero or negative for remnant distances below 650 pc (Salvesen et al. 2009). Also a distance slightly greater than 1 kpc would yield a SN explosion energy near the canonical SN explosion energy of 10^{51} erg. Such a distance could also explain the failure by Welsh et al. (2002) to detect high-velocity Na I and Ca II line absorptions associated with the remnant in several stars located in the line-of-sight to the Cygnus Loop at distances up to 800 pc.

If one or both of the two stars we have identified truly lie inside the Cygnus Loop, then parallax measurements will finally provide us with an accurate distance to the remnant. The ESA parallax mission, GAIA, which can measure parallax values down to 24 micro-arcseconds, is capable of providing this information.

Finally, we note that Boubert et al. (2017), who searched for runaway former companions of the progenitors of nearby Galactic core-collapse supernova remnants which included the Cygnus Loop, identified a 2 solar mass A type star candidate runaway TYC 2688-1556-1. However, they assumed a Cygnus Loop distance of 0.54

kpc which, if our estimate of $\simeq 1$ kpc is correct, means this star is unlikely to be a runaway companion star associated with the Cygnus Loop SN.

REFERENCES

Ballet, J., Arnaud, M., & Rothenflug, R. 1984, A&A, 133, 357

Bessell, M. S., & Brett, J. M. 1988, PASP, 100, 1134

Blair, W. P., Sankrit, R., Raymond, J. C., & Long, K. S. 1999, AJ, 118, 942

Blair, W. P., Sankrit, R., & Raymond, J. C. 2005, AJ, 129, 2268

Blair, W. P., Sankrit, R., Torres, S. I., Chayer, P., & Danforth, C. W. 2009, ApJ, 692, 335

Bok, B. J., & Warwick, C. 1957, AJ, 62, 323

Boubert, D., Fraser, M., Evans, N. W., Green, D., & Izzard, R. G. 2017, arXiv:1704.05900

Braun, R., & Strom, R. G. 1986, A&A, 164, 208

Chamberlain, J. W. 1953, ApJ, 117, 399

Ciotti, L., & D'Ercole, A. 1989, A&A, 215, 347

Cox, D. P. 1972, ApJ, 178, 169

Cox, A. N. 2000 Allen's Astrophysical Quantities, 4th ed. Publisher: New York: AIP Press; Springer

de Boer, K. S., Tucholke, H.-J., & Schmidt, J. H. K. 1997, A&A, 317, L23

Dodorico, S., Dopita, M. A., & Benvenuti, P. 1980, A&AS, 40, 67

Dopita, M. A., Binette, L., Dodorico, S., & Benvenuti, P. 1984, ApJ, 276, 653

Ducati, J. R., Bevilacqua, C. M., Rembold, S. B., & Ribeiro, D. 2001, ApJ, 558, 309

Duncan, J. C. 1923, ApJ, 57,

1997, The Hipparcos Catalogue, ESA SP-1200

Falle, S. A. E. G., & Garlick, A. R. 1982, MNRAS, 201, 635

Fang, J., Yu, H., & Zhang, L. 2017, MNRAS, 464, 940

Fesen, R. A., Blair, W. P., & Kirshner, R. P. 1982, ApJ, 262, 171

Fesen, R. A., Kwitter, K. B., & Downes, R. A. 1992, AJ, 104, 719

Fesen, R. A., & Hurford, A. P. 1996, ApJS, 106, 563

Fujimoto, S.-i., Kotake, K., Hashimoto, M.-a., Ono, M., & Ohnishi, N. 2011, ApJ, 738, 61

Gaia Collaboration, Brown, A. G. A., Vallenari, A., et al. 2016, A&A, 595, A2

Gray, R. O., & Corbally, C., J. 2009, Stellar Spectral Classification by Richard O. Gray and Christopher J. Corbally. Princeton University Press

Garcia, B. 1989, Bulletin d'Information du Centre de Donnees Stellaires, 36, 27

Garrison, R. F., & Gray, R. O. 1994, AJ, 107, 1556

Green, G. M., Schlafly, E. F., Finkbeiner, D. P., et al. 2015, ApJ, 810, 25

Hester, J. J., Danielson, G. E., & Raymond, J. C. 1986, ApJ, 303, L17

Hester, J. J., Raymond, J. C., & Blair, W. P. 1994, ApJ, 420, 721

Høg, E., Fabricius, C., Makarov, V. V., et al. 2000, A&A, 355, L27

Hubble, E. P. 1937, Washington, D.C., Carnegie institution of Washington, 1937

Jaschek, C., & Gomez, A. E. 1998, A&A, 330, 619

Katsuda, S., Tsunemi, H., Kimura, M., & Mori, K. 2008, ApJ, 680, 1198

Katsuda, S., Tsunemi, H., Mori, K., et al. 2011, ApJ, 730, 24

Keenan, P. C. 1985, Calibration of Fundamental Stellar Quantities, 111, 121

Kimura, M., Tsunemi, H., Katsuda, S., & Uchida, H. 2009, PASJ, 61, 137

Kirshner, R. P. 1976, PASP, 88, 585

Kovalevsky, J. 1998, ARA&A, 36, 99

Landolt, A. U. 2013, AJ, 146, 131

Lang, K. R. 1992, Astrophysical Data I. Planets and Stars, Springer-Verlag Berlin Heidelberg New York, 140

Levenson, N. A., Graham, J. R., Hester, J. J., & Petre, R. 1996, ApJ, 468, 323

Levenson, N. A., Graham, J. R., Aschenbach, B., et al. 1997, ApJ, 484, 304

Levenson, N. A., Graham, J. R., Keller, L. D., & Richter, M. J. 1998, ApJS, 118, 541

Mamajek, E., 2017, http:www.pas.rochester.edu/~emamajek

Martini, P., Stoll, R., Derwent, M. A., et al. 2011, PASP, 123, 187

Mathewson, D. S., & Clarke, J. N. 1972, ApJ, 178, L105

McCray, R., & Snow, T. P., Jr. 1979, ARA&A, 17, 213

McKee, C. F., & Cowie, L. L. 1975, ApJ, 195, 715

Medina, A. A., Raymond, J. C., Edgar, R. J., et al. 2014, ApJ, 791, 30

Massey, P., & Gronwald, C. 1990, ApJ, 358, 344

Minkowski, R. 1958, Reviews of Modern Physics, 30, 1048

Miyata, E., Tsunemi, H., Pisarski, R., & Kissel, S. E. 1994, PASJ, 46, L101

Miyata, E., Tsunemi, H., Kohmura, T., Suzuki, S., & Kumagai, S. 1998, PASJ, 50, 257

Miyata, E., & Tsunemi, H. 1999, ApJ, 525, 305

Oke, J. B. 1974, ApJS, 27, 21

Oort, J. H. 1946, MNRAS, 106, 159

Osterbrock, D. E. 1958, PASP, 70, 180

Osterbrock, D. E., & Ferland, G. J. 2006, Astrophysics of gaseous nebulae and active galactic nuclei, 2nd. ed. by D.E. Osterbrock and G.J. Ferland. Sausalito, CA: University Science Books

Parker, R. A. R. 1967, ApJ, 149, 363

Patnaude, D. J., Fesen, R. A., Raymond, J. C., et al. 2002, AJ, 124, 2118

Pickles, A. J. 1998, PASP, 110, 863

Preite Martinez, A. 2011, A&A, 527, A55

Raymond, J. C. 1979, ApJS, 39, 1

Raymond, J. C., Hartmann, L., Black, J. H., Dupree, A. K., & Wolff, R. S. 1980, ApJ, 238, 881

Raymond, J. C., Black, J. H., Dupree, A. K., & Hartmann, L. 1981, ApJ, 246, 100

Raymond, J. C., Edgar, R. J., Ghavamian, P., & Blair, W. P. 2015, ApJ, 805, 152

Rappaport, S., Doxsey, R., Solinger, A., & Borken, R. 1974, ApJ, 194, 329

Ross, F. E. 1931, ApJ, 74, 85

Salvesen, G., Raymond, J. C., & Edgar, R. J. 2009, ApJ, 702, 327

Sakhibov, F. K., & Smirnov, M. A. 1983, Soviet Ast., 27, 395

Schlafly, E. F., Green, G., Finkbeiner, D. P., et al. 2014, ApJ, 789, 15

Schonberner, D., & Drilling, J. S. 1984, ApJ, 278, 702

Scoville, N. Z., Irvine, W. M., Wannier, P. G., & Predmore, C. R. 1977, ApJ, 216, 320

Skrutskie, M. F., Cutri, R. M., Stiening, R., et al. 2006, AJ, 131, 1163

Shull, P., Jr., & Hippelein, H. 1991, ApJ, 383, 714

Shull, J. M., & McKee, C. F. 1979, ApJ, 227, 131

Sutherland, R. S., Bicknell, G. V., & Dopita, M. A. 2003, ApJ, 591, 238

Tsunemi, H., Katsuda, S., Nemes, N., & Miller, E. D. 2007, ApJ, 671, 1717

Uchida, H., Tsunemi, H., Katsuda, S., et al. 2009, PASJ, 61, 503

Walsh, D., & Brown, R. H. 1955, Nature, 175, 808

Wegner, W. 2006, MNRAS, 371, 185

Welsh, B. Y., Sallmen, S., Sfeir, D., & Lallement, R. 2002, A&A, 391, 705

Wolf, M. 1923, Astronomische Nachrichten, 219, 109

Zwicky, F. 1940, Reviews of Modern Physics, 12, 66